A Nanoparticle Approach towards Morphology Controlled Organic Photovoltaics (OPV)

Andersen, Thomas Rieks; Yan, Quanxiang; Larsen-Olsen, Thue Trofod; Søndergaard, Roar; Li, Qi; Andreasen, Birgitta; Norrman, Kion; Jørgensen, Mikkel; Yue, Wei; Yu, Donghong

Total number of authors:
13

Published in:
Polymers

Link to article, DOI:
10.3390/polym4021242

Publication date:
2012

Document Version
Publisher's PDF, also known as Version of record

Polymers **2012**, *4*, 1242-1258; doi:10.3390/polym4021242

OPEN ACCESS

polymers

ISSN 2073-4360

www.mdpi.com/journal/polymers

Article

A Nanoparticle Approach towards Morphology Controlled Organic Photovoltaics (OPV)

Thomas R. Andersen [1], Quanxiang Yan [2,3], Thue T. Larsen-Olsen [1], Roar Søndergaard [1], Qi Li [2], Birgitta Andreasen [1], Kion Norrman [1], Mikkel Jørgensen [1], Wei Yue [3], Donghong Yu [3], Frederik C. Krebs [1], Hongzheng Chen [2] and Eva Bundgaard [1,*]

[1] Department of Energy Conversion and Storage, Technical University of Denmark, Frederiksborgvej 399, DK-4000 Roskilde, Denmark; E-Mails: tria@dtu.dk (T.R.A.); thols@dtu.dk (T.T.L.-O.); rosq@dtu.dk (R.S.); baan@dtu.dk (B.A.); kino@dtu.dk (K.N.); mijq@dtu.dk (M.J.); frkr@dtu.dk (F.C.K.)

[2] State Key Laboratory of Silicon Materials, MOE Key Laboratory of Macromolecule Synthesis and Functionalization and Department of Polymer Science and Engineering, Zhejiang University, Hangzhou 310027, China; E-Mails: yqx0116@163.com (Q.Y.); 11210440008@fudan.edu.cn (Q.L.); hzchen@zju.edu.cn (H.C.)

[3] Department of Biotechnology, Chemistry, and Environmental Engineering, Aalborg University, Sohngaardsholmsvej 57, DK-9000 Aalborg, Denmark; E-Mails: wy@bio.aau.dk (W.Y.); yu@bio.aau.dk (D.Y.)

***** Author to whom correspondence should be addressed; E-Mail: evbu@dtu.dk; Tel.: +45-4677-5498; Fax: +45-4677-4791.

Received: 16 April 2012; in revised form: 24 May 2012 / Accepted: 4 June 2012 / Published: 11 June 2012

Abstract: Silicon nano-particles grafted with two different organic oligomers were prepared; the oligomers used were a phenylene-vinylene (PV) oligomer and a 3,3'''-didodecylquaterthiophene. The graftings were performed by the use of two different functional groups, the PV oligomer was grafted by a hydroxyl-group in the form of a phenol and a lithium derivative was used to graft the 3,3'''-didodecylquaterthiophene. The morphology and size of the grafted particles were analyzed by atomic force microscopy (AFM) and the extent of the grafting was analyzed by NMR. Organic photovoltaics with normal geometry (ITO/PEDOT:PSS/active layer/Al) were prepared using these materials as a donor and phenyl-C61-butyric acid methyl ester ([60]PCBM) as the acceptor and yielded a power conversion efficiency (PCE) of 0.27%, an open circuit voltage (V_{OC}) of

0.93 V, a short circuit current density (J_{SC}) of 0.89 mA/cm^2, and a fill factor (FF) of 32.5% for a lead device with an active area of 0.25 cm^2.

Keywords: organic photovoltaics; silicon nano-particles; morphology control

1. Introduction

Organic photovoltaics (OPV) have in the past decade been the subject of increasing interest, primarily due to its potential as a low cost sustainable energy source [1–5]. The best performing OPV devices have been prepared with the bulk heterojunction (BHJ) architecture in the photoactive layer, which is a blend of a p-type (donor) and an n-type material (acceptor) [2]. It is well-known that the morphology of the photoactive layer in a BHJ has a large influence on the power conversion efficiency (PCE) [3–5]. This is mainly ascribed to: (1) the crystallinity of the organic materials, where a higher degree of crystallinity enhances the carrier transport through higher mobility and thus increases the efficiency [4,6], and (2) the phase separation between the donor and acceptor materials, which should form a continuous entangled network of the donor and acceptor with domain sizes similar to the exciton diffusion length of about 10 nm [4]. Thus, ensuring the optimal conditions for exciton disassociation is directly correlated with the short circuit current [2]. Morphology optimization is often attempted by self assembly; the two most widely used methods are thermal annealing and solvent annealing [4,5]. Thermal annealing is a post production heat-treatment of the active layer, which often promotes the semi-crystalline components in the active layer to form a more ordered packing or crystals if possible [4]. The technique of solvent annealing uses a solvent with a higher boiling point thereby decreasing the rate of evaporation, which allows larger domains to form [5]. This can lead to an improvement of the interpenetration between the donor and acceptor and usually also an increased order within the polymer domains [5]. Another method for this optimization is the use of additives such as 1,8-octanedithiol, 1,8-diiodooctane etc. This method is similar to solvent annealing since the additive has a higher boiling point than the main solvent and provides better solubility for one of the components. In the case of 1,8-octanedithiol, 1,8-diiodooctane and 1-chloronaphthalene the solubility of PCBM is larger than a donor-polymer such as poly(3-hexylthiophene) (P3HT) [4] and this results in the formation of large domains of PCBM. These methods are generally easy and of low cost and therefore often used. However, the morphologies obtained are often not stable for a long time [6,7]. They have a tendency to form larger domains causing the overall performance to drop especially after exposure to heat [6,7]. A couple of methods for overcoming the bulk diffusion have been presented. The first method is to cross link either the donor- or the acceptor-molecules within the bulk, thereby forming a rigid network which makes the diffusion more limited [8,9]. A drawback to this method is that the modifications within the active layer are carried out during or after fabrication of the device, thus risking residual products or initiators from the cross-linking to be contained within the film, which could potentially decrease the device life-time.

A radically different approach is to use preformed nano-particles as templates for the morphology, which is the focus of this paper. Instead of relying on a random self-assembly process as described above, this approach uses nano-particles of 15–20 nm, thus automatically ensuring an optimal

interpenetrating network of donor and acceptor. The approach was introduced by Kiriy *et al.* [10–12], where P3HT is polymerized from the surface of silica (SiO_2) nano-particles, thereby achieving polymer chains that are covalently grafted onto the surface of nano-particles. This eliminates diffusion and locks the morphology. A disadvantage to this method is the introduction of silica within the active layer which results in very limited contribution to the absorption of photons leading to thicker active layers to ensure the same absorption thereby risking a decrease in fill factor [13].

In this paper we report a pathway to overcome the lack of absorption from the nano-particle approach; we exchanged the silica with silicon nano-particles in our study. This should also ensure a stable morphology, but more importantly, increases the absorption since the absorption from silicon is much greater than for silica towards longer wavelengths. The absorption of the silicon nano-particles should theoretically be size dependent [14], *i.e.*, larger nano-particles result in longer wavelengths of the absorbing light. For the organic grafting agent two different organic molecules were used; a PV oligomer (**1**) presented by Søndergaard *et al.* [15], and 3,3'''-didodecylquaterthiophene (**2**) (see Scheme 1). The latter was used to compare the nano-particles with current materials used in OPV devices.

Scheme 1. Preparation of the silicon nano-particles (NP) and the grafting of the nano-particles with compounds **1** and **2**.

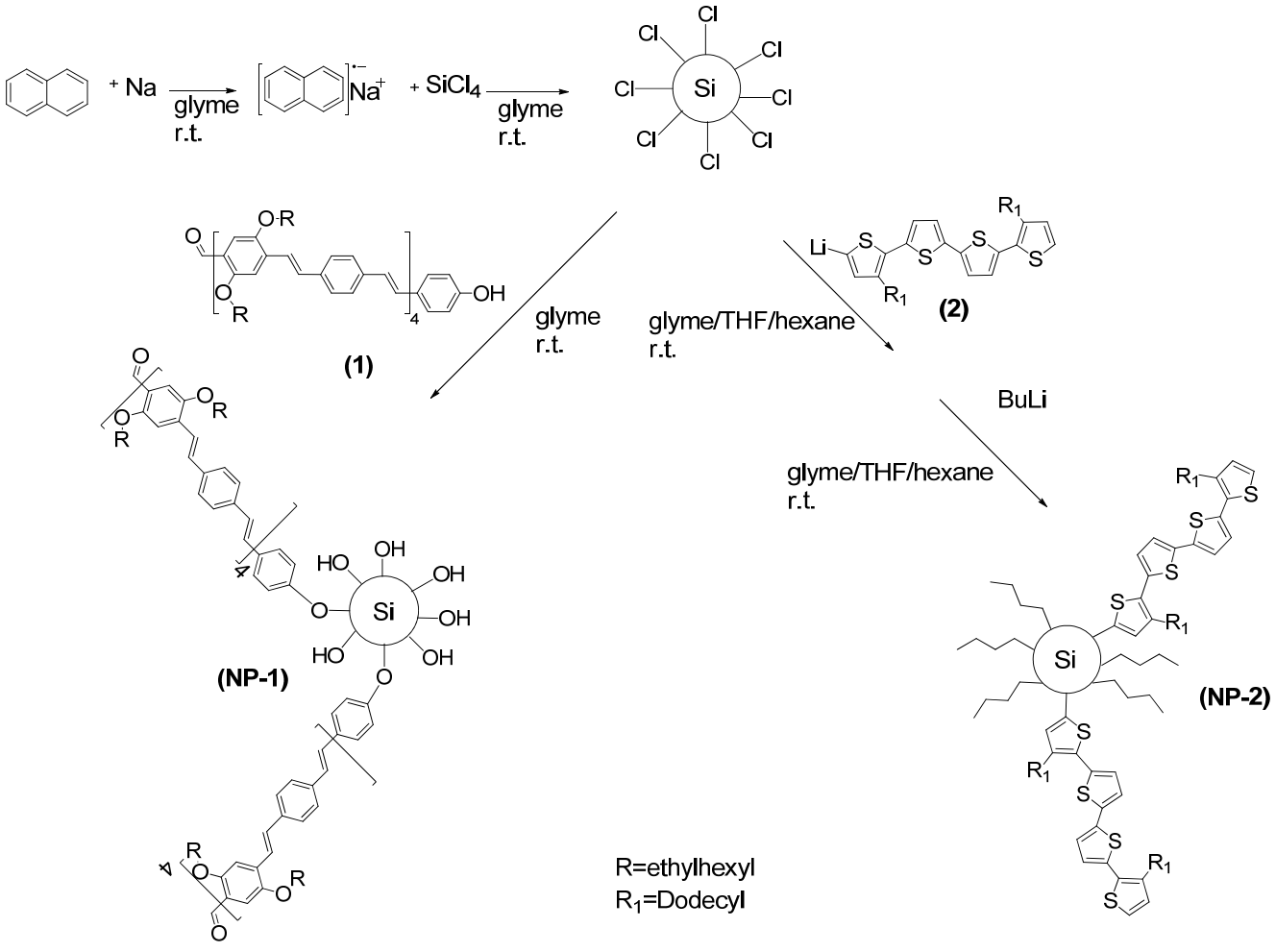

2. Experimental Section

2.1. Preparation of Nano-Particles

All chemicals for the preparation of the silicon nano-particles were purchased from Sigma-Aldrich, and were used as received except glyme which was dried over sodium prior to use. The PV oligomers were prepared as describe by Søndergaard *et al.* [15]. All reactions were carried out under an argon atmosphere.

The Si-nano particles used for **NP-1** and **NP-2** were prepared as described by Baldwin *et al.* [16] and Baldwin *et al.* [17], respectively.

NP-1: Sodium (0.1 g, 4.3 mmol) was added to a dry glyme solution (5 mL) and naphthalene (0.35 g, 2.7 mmol) and stirred for 3 hours after which a black yellowish solution of sodium naphthalide was obtained. This solution was added to $SiCl_4$ (99.9%, 0.08 mL, 0.7 mmol) in dry glyme solution (30 mL) and stirred for 30 min. after which the organic grafting agent (**1** (see Scheme 1), 100 mg, 0.05 mmol) was added and the reaction mixture was stirred for 2 hours. The solvent was removed under reduced pressure; the residue was dissolved in heptane and washed with water. During the washing a red solid phase was formed near the water/heptane interface which was filtered off and was verified by ^{1}H-NMR to be unreacted grafting agent. The organic phases were collected and the solvent was removed under reduced pressure, the residue was heated to 90 °C also in vacuum to remove residual naphthalene. The solid was extracted with chloroform and heptane, and when these were combined precipitation occurred. The suspension was filtered to give the functionalized nano-particles (**NP-1**) as a sticky red solid (108 mg).

^{1}H NMR spectra of compound **1** and **NP-1** are shown in Figure 1.

Figure 1. ^{1}H-NMR spectra of compound **1** and **NP-1** measured in $CDCl_3$.

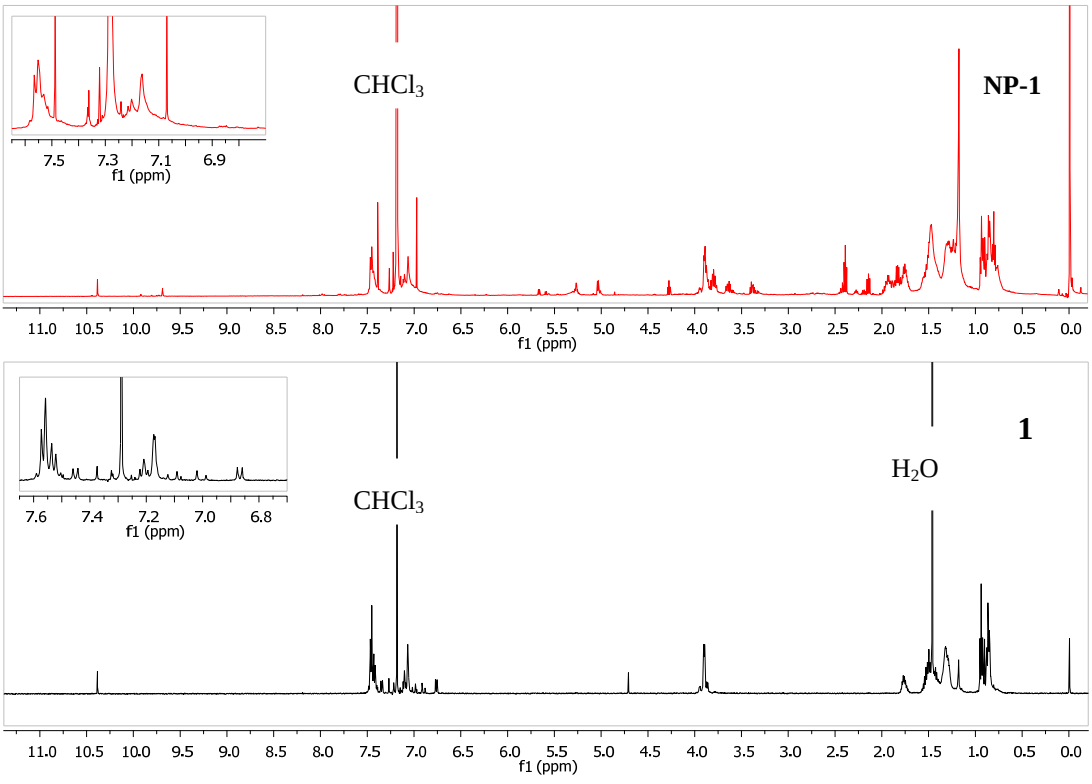

NP-2: Sodium naphthalide was prepared from sodium (0.36 g, 15.7 mmol) and naphthalene (1.48 g, 11.5 mmol) in dry glyme (20 mL)). After stirring over night $SiCl_4$ (0.52 g, 4.5 mol) was added drop-wise into the dry glyme solution of sodium naphthalide. The color of the suspension changed from dark yellow to deep brown. After stirring for 2 hours, 5-lithio-3,3'''-didodecylquaterthiophene (80 mg 0.12 mmol) (prepared from 3,3'''-didodecylquaterthiophene **2** and n-butyl lithium in 10 mL THF) was added. Excess of n-butyl lithium was added to the reaction-flask to passivate silicon nano-particles with butyl groups. After vigorously stirring overnight, the solvent was removed under reduced pressure and naphthalene was removed by continuously purging N_2 into the flask in a heating mantle under vacuum for 12 hours. The resulting yellow solid was extracted with hexane and washed three times with distilled water. The hexane layer was collected and solvent was removed in vacuum to give the functionalized nano-particles (**NP-2**) as a waxy yellow solid (67 mg).

^{1}H NMR spectra of compound **2** and **NP-2** are shown in Figure 2.

Figure 2. The ^{1}H-NMR-spectra of compound **2** and **NP-2** measured in $CDCl_3$.

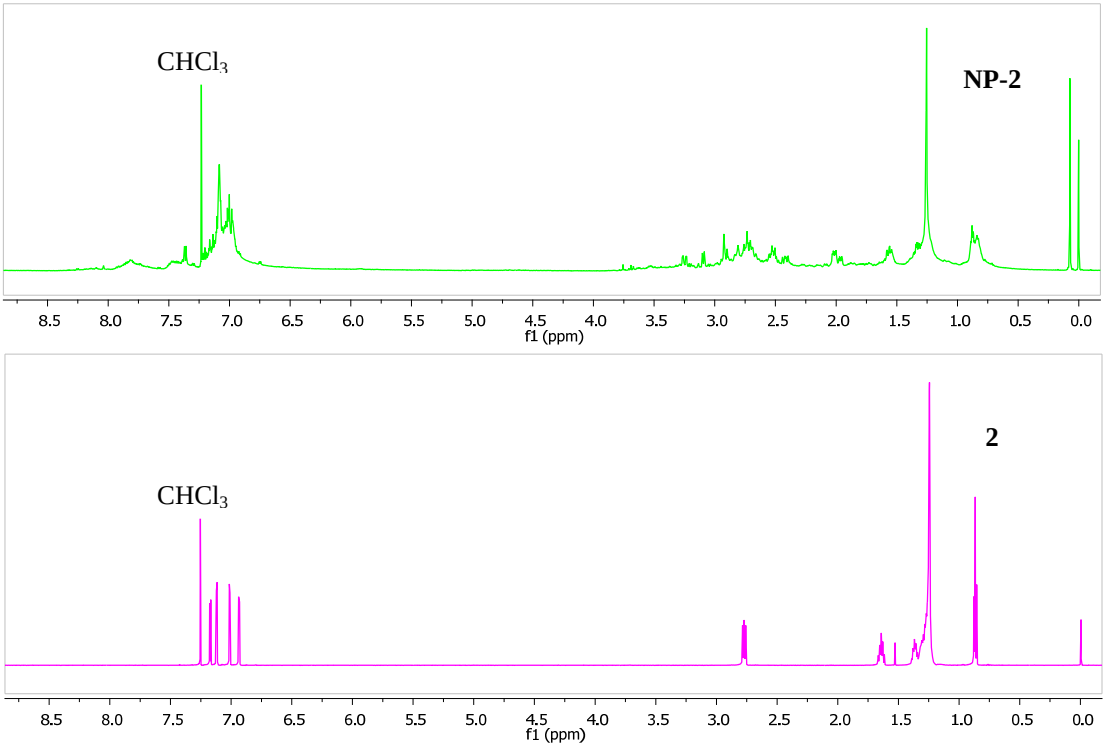

2.2. UV-Vis Spectroscopy

The UV-Vis spectroscopy in solution was carried out on a Varian Cary50 Bio UV-Visible Spectrophotometer (Agilent Technologies, USA) and in film on a PharmaSpec UV-1700 (SHIMADZU, Japan).

2.3. Device Fabrication and Characterization

Photovoltaic devices were fabricated by spin coating PEDOT:PSS (Clevios PVP.Al 4083, Heraeus) (3000 rpm) on top of pre-cleaned, patterned indium tin oxide (ITO) on glass slides and then baked at 140 °C for 5 min. The active layer was deposited by spin coating a mixture of the functionalized

nano-particles (**NP-1** or **NP-2**) and [60]PCBM in chloroform (1:1, 20 mg/mL). The back electrode consisting of about 100 nm aluminum was deposited by vacuum evaporation. Some samples were annealed at 140 °C for 2 min. I-V measurements were carried out with a Keithley (2440) as a source meter under a solar simulator from Steuernagel (solar constant KHS 575) with 1000 W/m^2, AM1.5G. The active area of the devices was 0.25 cm^2 and the thickness of the active layer was determined by atomic force microscopy (AFM).

2.4. Atomic Force Microscopy

AFM imaging of the active layers was performed on an N8 NEOS (Bruker Nano GmbH, Herzogenrath, Germany) operating in an intermittent contact mode using PPP-NCLR cantilevers (NANOSENSORS, Neuchatel, Switzerland). Images were recorded at a scan speed of 1 line/sec. The images were analyzed using the image processing software package SPIP 5.1.5 (Image Metrology A/S, Hørsholm, Denmark) for the height measurements, and the particle size determination. AFM images of nanoparticles were performed in semi-contact mode on a NTEGRA life instrument (NT-MDT), with an Olympus AC240TS cantilever at a resonance frequency of 140 kHz. WSxM Program was used for image data processing [16], samples were prepared by drop-casting a dilute solution of nano-particles in chlorobenzene on to a substrate of Muscovite Mica (size: 9.5 mm Diameter, thickness: 0.15–0.21 mm, Electron Microscopy Science).

3. Results and Discussion

3.1. Fabrication of Nano-Particles

The grafting technique used to graft the organic oligomers onto the silicon nano-particles, has previously been reported [17–19]. The grafting reactions were carried out by nucleophilic substitution by organic materials containing a hydroxyl-group as a final step in the preparation of the nano-particles, but also by the use of lithiated-molecules.

The preparation of silicon nano-particles presented two major challenges. In previously published work [16,20] the nano-particles were washed with water as part of the purification, however, in this work an impurity was observed, which was evident from a peak around 7 ppm in the ^{1}H-NMR-spectrum (Figure S1 in Supporting Information). This can be overcome by employing sublimation as the primary method for removal of naphthalene. This approach was developed using silicon nano-particles with meta-cresol as the grafting agent. The ^{1}H-NMR spectra of these test reactions can be seen in the Supporting Information (Figure S1).

The second challenge that was discovered during the preparation of the nano-particles was the irreversible adsorption of nano-particles onto the glassware and aggregation of nano-particles when solvents were removed during purification, which unfortunately led to an unavoidable and significant loss of material.

The ^{1}H-NMR spectra of compound **1** and **NP-1** are given in Figure 1. Some of the key features in the spectrum of **NP-1** originating from compound **1** are very similar after grafting. In particular, this includes the peaks from 6.7 to 7.7 ppm due to protons in the aromatic moieties but also from 0.7 to 2 ppm that are due to protons in the aliphatic side chains. However, the signal from the phenol-group

(4.85 ppm) has disappeared as expected; a small singlet at 4.95 ppm remains that could be the signal from compound **1** where the phenol has not reacted. However, this peak integrates only to 0.14 against the aldehyde-group, which leads us to the conclusion that at least 85% of compound **1** within the sample is grafted to the surface of the nano-particles. Besides these results the spectra between 6.7 ppm to 7.7 ppm are less defined which should be expected by the lower mobility induced by the grafting. These results correlate well with results already published by Ruckenstein *et al.* [21] where it is shown that grafting of silicon nano-particles with an organic agent results in very little, if any, shifts in the NMR-spectra for the organic grafting agent.

In contrast to **NP-1**, the ^{1}H-NMR spectrum of **NP-2** shows very broadened signals in the regions compared to the spectrum of **2** (see Figure 2). This broadening of the signals is probably an effect of the greatly diminished mobility of the quarterthiophene molecule after it has been grafted onto the nano-particle. It is not possible to find which ^{1}H signal has disappeared due to the grafting, partially because of the presence of an impurity giving rise to signals in the aromatic region. Signals in the aliphatic regions from both **2** and butyl groups, which were also grafted, are visible.

3.1.1. Morphology and Size Characterization

AFM was used to measure the size of the Si nano-particles. The AFM image of **NP-1** (see Figure 3) shows a monolayer of spherical particles which have a tendency to aggregate into clusters. The size distribution of the particles shows the main particle size to be 7.0 (±1.8) nm for **NP-1** and 6.8 (±3.8) nm for **NP-2**, which is about half the size of what is thought to be the optimal size, *i.e.*, 15–20 nm.

Figure 3. AFM image of **NP-1** coated on mica by drop casting from a diluted solution in chlorobenzene (**left**) and the size distribution of the particles determined by their height (**right**).

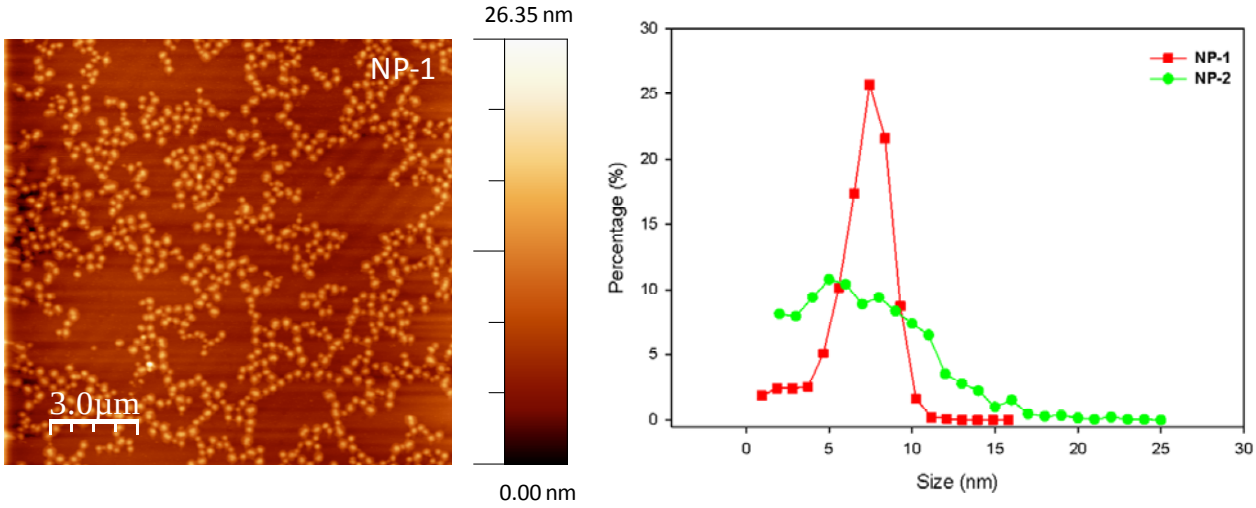

3.2. Optical Properties

The normalized absorption spectra for all materials are given in Figure 4 for compound **1** and **NP-1** and Figure 5 for compound **2** and **NP-2**, respectively.

Figure 4. Absorption spectra of compound **1** and **NP-1** in $CHCl_3$.

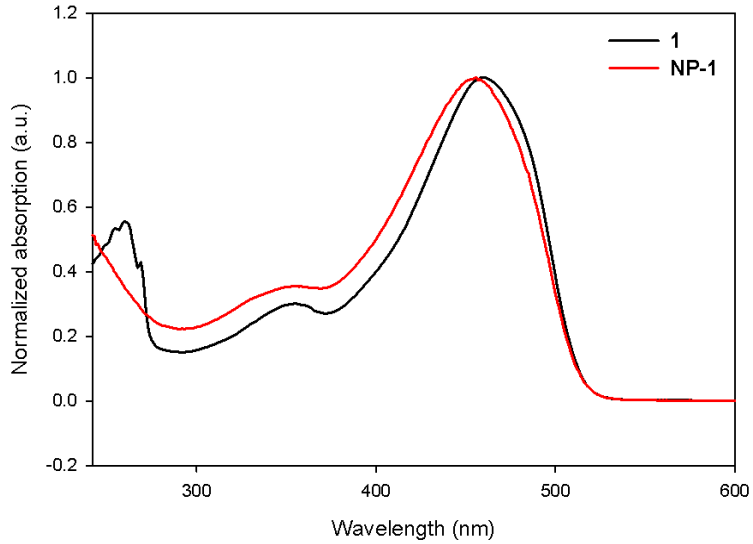

Figure 5. The absorption of compound **2** and **NP-2** in CH_2Cl_2.

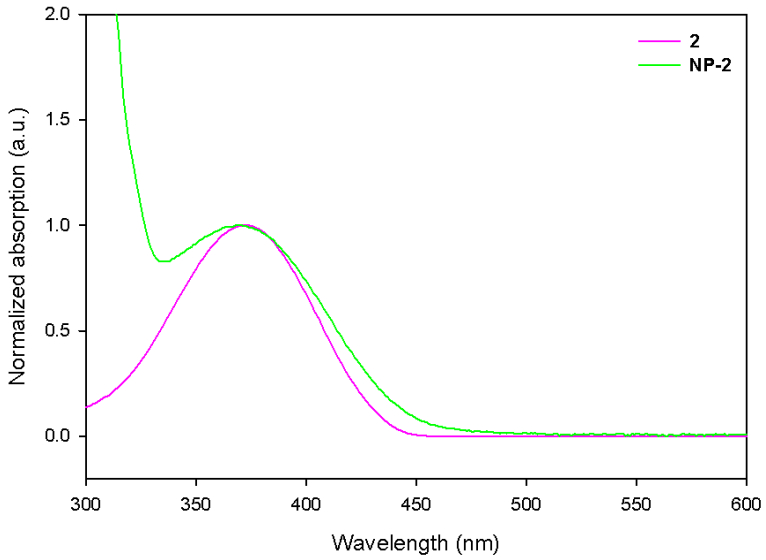

The absorption of **NP-1** in a chloroform solution is very similar to that of compound **1**. There is a slight difference in the maximum absorption where **NP-1** seems to have a small blue-shift (from 460 nm for **1** to 456 nm for **NP-1**). There is also a difference at low wavelengths, where the absorption from **1** decreases after peaking at 260 nm and the absorption from **NP-1** continues to increase. The variation is ascribed to the absorption of the Si-nano-particles.

The absorption spectra for compound **2** and **NP-2** have some similarities. As observed for **1** and **NP-1**, a very small blue-shift (from 373 to 370 nm) can also be observed for the max absorption in the range from 350–450 nm after grafting. There is, however, some difference in the spectra at the edge absorption, where **2** absorbs from 433 nm, **NP-2** absorbs from 443 nm. The major difference is the point at lower wavelengths (less than 340 nm) which is ascribed to absorption of the Si-nano particles (see Supporting Information Figure S2). The difference between **NP-1** and **NP-2** is ascribed to **NP-2** containing larger nano-particles, *i.e.*, up to above 15 nm, and **NP-1** only containing nano-particles up to 10 nm (see Figure 3).

3.3. Device Performance

OPV devices were prepared as described in the experimental section and measured under artificial sun (1000 W/m^2, AM1.5G). The IV data are summarized in Figure 6 and Table 1.

The devices prepared with compound **1** and **NP-1** both show clear solar cell characteristics (Figure 6). When examining the devices carefully, it became clear that there was a large difference in absorption for **Device 1** and **Device 4**. This difference was investigated by the optical reflectance of the two devices, which was measured using the back electrode as a mirror.

Figure 6. I-V-curves for the two different device types, **Device 1** and **Device 4**.

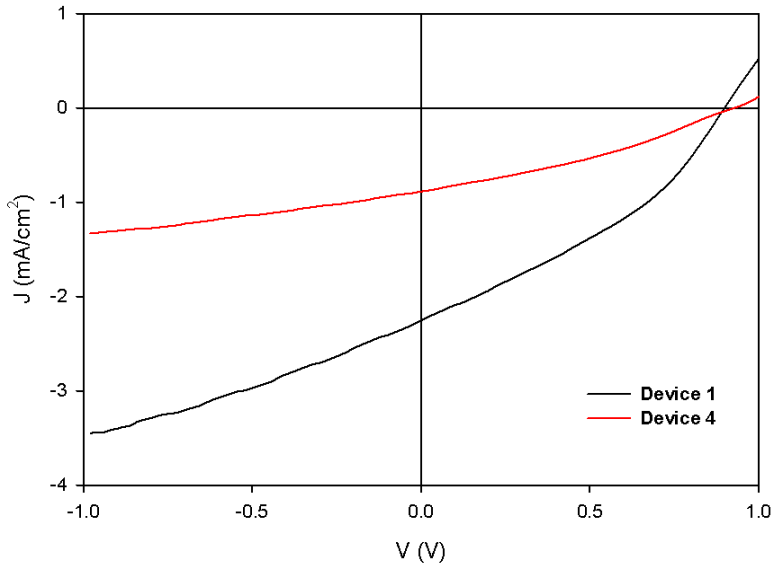

Table 1. A collection of the data obtained for all the devices, *i.e.*, thickness, absorption in the active layer, reflectance, device material, and photovoltaic properties: PCE, open circuit voltage (V_{OC}), short circuit current density (J_{SC}), and fill factor (FF)) obtained for the devices with the geometry glass/ITO/PEDOT:PSS/donor-[60]PCBM (1:1 w/w, 20 mg/mL)/Al and an active area of the devices of 0.25 cm^2. The testing conditions were AM1.5G (Xe-lamp, 1000 W/m^2, 85 ±5 °C). The thicknesses were determined by AFM as reported previously [22].

Device	Matertial	Thickness (nm)	Abs. [a]	Reflec. [b] (%)	J_{SC} (mA/cm^2)	V_{OC} (V)	FF (%)	PCE (%)
1	**1**	232	NA	40	2.26	0.90	35.0	0.71
2	**1**	146	0.451	NA	1.77	0.54	30.5	0.29
3	**1**	63	0.181	NA	2.15	0.05	25.5	0.03
4	**NP-1**	124	NA	10	0.89	0.93	32.5	0.27
5	**NP-1**	141	0.243	NA	0.44	0.76	28.0	0.09
6	**NP-1**	101	0.130	NA	0.70	0.41	29.8	0.09

[a] Light absorption in the active layer given as the peak absorption in the range 400–530 nm; [b] Reflectance of the device given as the drop in reflectance for approx. 600 nm to 470 nm.

The reflectance (Figure 7) for **Device 1** drops from 60% to approximately 20% at the wavelength where **1** absorbs (400–530 nm), whereas the reflection for **Device 4** only drops from 55% to around 45%. This large difference in reflectance could be the main reason for the poorer J_{SC} for **Device 4** in comparison with **Device 1**. To further determine which influence the introduction of silicon nano-particles have on the OPV devices, another batch of devices were prepared with the aim of creating active layers with similar absorption in the range of 400–530 nm.

Figure 7. Reflection spectra of **Device 1** and **Device 4**.

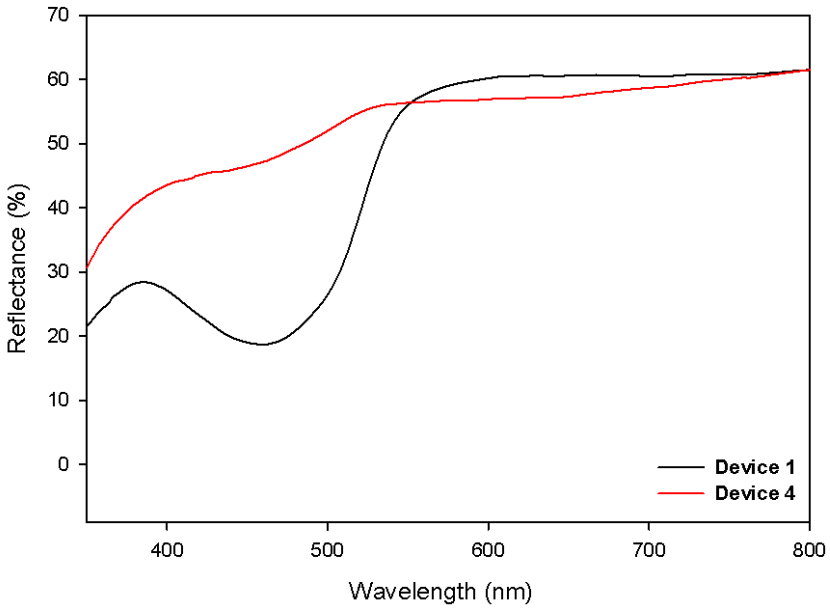

The absorption curves of the active layers and the I-V curves for these devices can be found in Supporting Information. The data is summarized in Table 1.

For the absolute absorptions, as illustrated in Figure 8 and summarized in Table 1, it is seen that **Device 5**, **Device 6**, and **Device 3** to a large extent have comparable absolute absorptions and only a small difference is observed: **Device 6** < **Device 3** < **Device 5**. In addition to these observations the position of the peak absorption between 400 and 600 nm are as for the solution still very similar (Figure 8). The phenomena was reported by Senkovskyy *et al.* [10] who ascribe it to an effect of grafting on small nano-particles which leads to distant organic chains thereby allowing them to have a similar behavior as "free" molecules.

The I-V curves (shown in Figure 9 and summarized in Table 1) obtained from the device prepared with the absorptions from Figure 8, display a device prepared with **1** (**Device 2**) as the champion device, whereas **Device 5** and **Device 6** despite the difference in absorption have very similar performance. **Device 3** is very poorly performing; this is ascribed to shorts in the very thin active layer (63 nm).

Figure 8. The absorption for the active layers in **Devices 2**, **3**, **5**, and **6**.

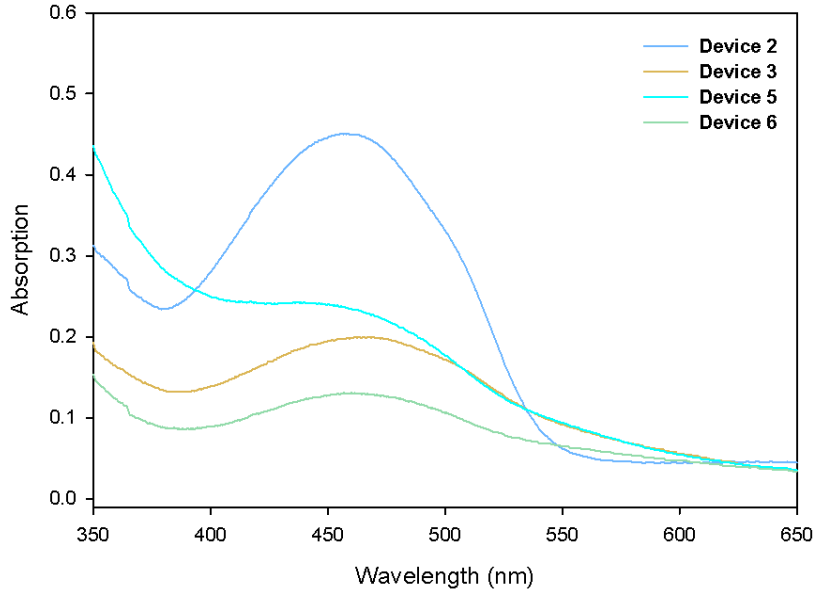

Figure 9. I-V curves for the **Devices 2**, **3**, **5**, and **6**.

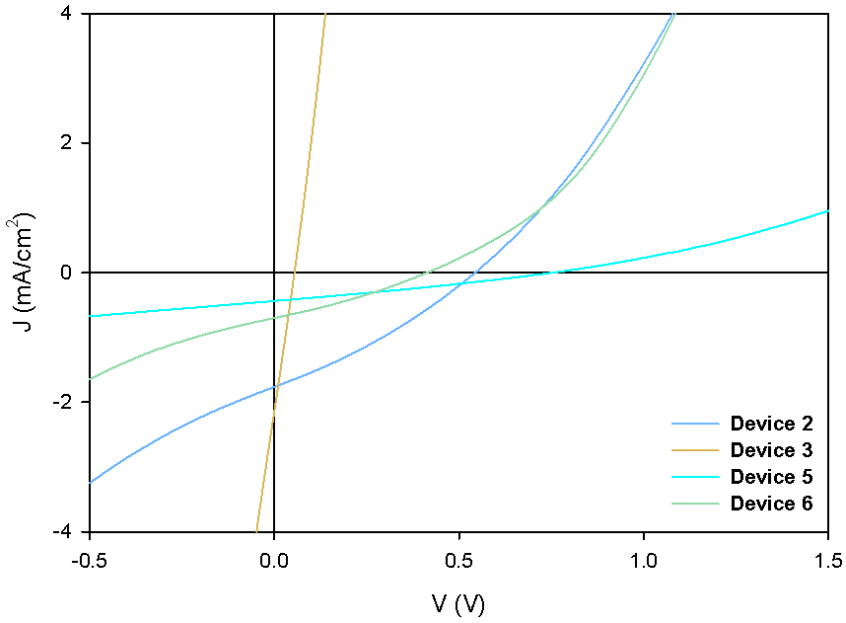

Another parameter for comparison between the fabricated devices is the thickness of the active layer. From Table 1 it can be found that **Device 2** based on **1** and **Device 5** based on **NP-1** have very similar thicknesses with 146 and 141 nm, respectively. Although the device thicknesses are very similar the rest of the device characteristics are very different; the absolute absorption for **Device 2** is almost twice the absorption of **Device 5** and the PCE of 0.29% is about three times as high as for **Device 5** which is mainly ascribed to a larger J_{SC}. This would perhaps be less pronounced if the silicon nano-particles had a size in the range of 15–20 nm, which could increase the maximum wavelength at which they absorb.

Previously it has been reported that Si nano-particles have a strong tendency to undergo oxidation when exposed to ambient air [23]. This oxidation would lead to undesirable properties or a least

decrease the desired properties of the nano-particles. As an example, an insulating SiO_2 layer can be formed on the surface of the nano-particle [24]. Such an oxidation could be an additional explanation for the poorer performance of the devices containing Si nano-particles.

The I-V curves from the devices prepared with **2** or **NP-2** and [60]PCBM showed no or very little photovoltaic properties (see Supporting Information, Figure S3); the best performing device was **NP-2** annealed with a PCE of 0.001%.

3.3.1. Morphology of Active Layers

The AFM topography images of the active layers in **Device 2** and **Device 5** are shown in Figure 10. The images illustrate almost two different morphologies. **Device 2** seems to have a more homogeneous (smooth) surface with naturally occurring surface roughness containing no high peaks or pinholes. By comparison, the active layer in **Device 5** is covered with pinholes, which greatly affect the resulting surface morphology. The formation of pinholes could be one of the explanations as to why the devices containing **NP-1** perform poorly in comparison with the devices containing **1**.

Figure 10. AFM topography images of the active layers of **Device 2** and **Device 5** with their respective height difference (z range) and the calculated surface roughness (S_a). The imaging was conducted on the active layer of the fully assembled devices.

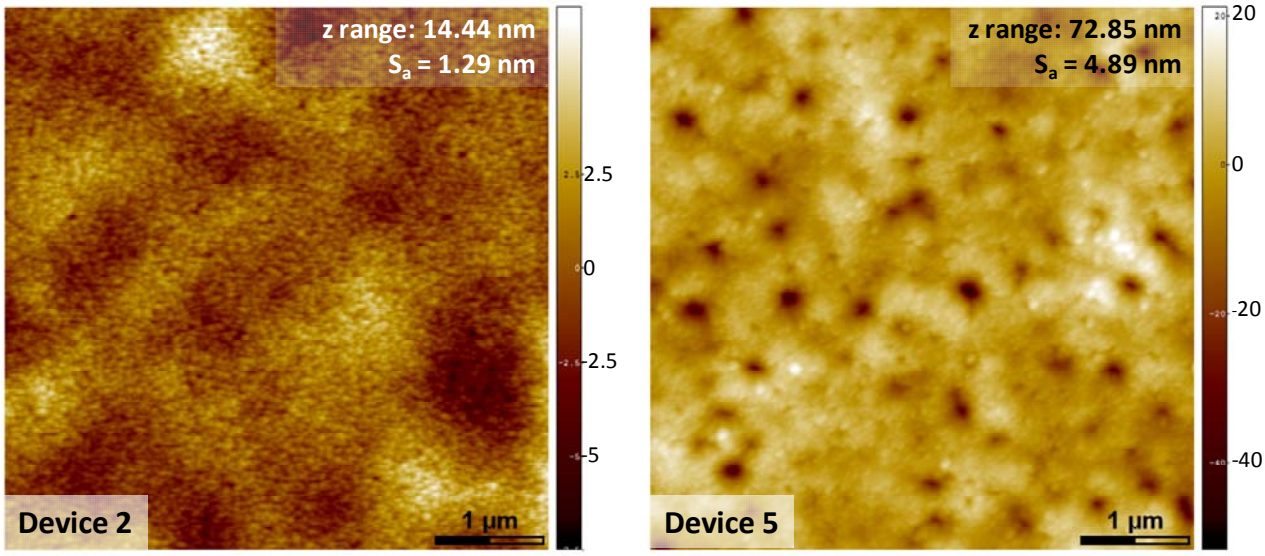

4. Conclusions

Silicon nano-particles grafted with two different organic conjugated oligomers were prepared and the nano-particles were investigated by AFM and NMR to verify the creation of nano-particles and the grafting of oligomers. AFM analysis showed nano-particles with sizes in the range of 5–10 nm for **NP-1** and in the range 4–15 nm for **NP-2**. NMR analysis showed a loss of the phenol-signal for **NP-1,** which shows successful grafting for **1**, for **NP-2** a significant broadening in the signal of the aromatic proton occurred which comes from the greater immobility after grafting. Photovoltaic devices were prepared with [60]PCBM. Devices containing nano-particles with compound **1** grafted on (**NP-1**)

yielded a power conversion efficiency of 0.27%, which is significantly lower than for the non grafted **1** (PCE 0.71%). However, reflection studies of the active layers showed an absorption in the active layer of the devices prepared with **NP-1**, which were much lower than for devices prepared with **1**. Another set of cells were prepared with similar absorption of **1** and **NP-1** in the active layer. Here the cells containing silicon nano-particles were still poorer performing. The devices prepared with 3,8-didodecylquaterthiophene (**2**) as the grafted oligomer and [60]PCBM showed very little photovoltaic properties after annealing whereas the devices prepared with **2** and [60]PCBM show no photovoltaic properties.

In this paper we have described a method to control the morphology of the active layer in an OPV device by grafting silicon nano-particles with different oligomers. There is, however, some drawbacks to this method, *i.e.*, it is very difficult to purify the grafted nano-particles and there is a great loss of material during this purification due to aggregation and adsorption to glassware. The devices prepared from the nano-particles showed a decrease in the photovoltaic performance compared to devices prepared with non-grafted oligomer. This drop in performance could be due to the formation of pinholes within the nano-particle film, even with relative thick films (141 nm). Furthermore, the drop in performance could be due to oxidation of the nano-particles surface, which could be overcome by carrying out the synthesis, fabrication, and measurements in a glove box.

Acknowledgments

This work was financially supported by the Danish National Research Foundation (DNRF) and the National Natural Science Foundation of China (NSFC) (Grants 50990063 and 51011130028). We would also like to gratefully acknowledge support from the DNRF and the NSFC for the Danish-Chinese Center for Organic based Photovoltaic Cells, within which this work was performed.

References

1. Helgesen, M.; Søndergaard, R.; Krebs, F.C. Advanced materials and processes for polymer solar cell devices. *J. Mater. Chem.* **2010**, *20*, 36–60.
2. Cai, W.; Gong, X.; Cao, Y. Polymer solar cells: Recent development and possible routes for improvement in the performance. *Sol. Energy Mater. Sol. Cells* **2010**, *94*, 114–127.
3. Dennler, G.; Scharber, M.C.; Brabec, C.J. Polymer-fullerene bulk-heterojunction solar cells. *Adv. Mater.* **2009**, *21*, 1323–1338.
4. Peet, J.; Senatore, M.L.; Heeger, A.J.; Bazan, G.C. The role of processing in the fabrication and optimization of plastic solar cells. *Adv. Mater.* **2009**, *21*, 1521–1527.
5. Yang, X.; Loos, J. Toward high-performance polymer solar cells: The importance of morphology control. *Macromolecules* **2007**, *40*, 1353–1362.
6. Bertho, S.; Janssen, G.; Cleij, T.J.; Conings, B.; Moons, W.; Gadisa, A.; D'Haen, J.; Goovaerts, E.; Lutsen, L.; Mancaa, J.; Vanderzande, D. Effect of temperature on the morphological and photovoltaic stability of bulk heterojunction polymer:fullerene solar cells. *Sol. Energy Mater. Sol. Cells* **2008**, *92*, 753–760.

7. Paci, B.; Generosi, A.; Albertini, V.R.; Generosi, R.; Perfetti, P.; de Bettignies, R.; Sentein, C. Time-resolved morphological study of bulk heterojunction films for efficient organic solar devices. *J. Phys. Chem. C* **2008**, *112*, 9931–9936.
8. Griffini, G.; Douglas, J.D.; Piliego, C.; Holcombe, T.W.; Turri, S.; Fréchet, J.M.J.; Mynar, J.L. Long-term thermal stability of high-efficiency polymer solar cells based on photocrosslinkable donor-acceptor conjugated polymers. *Adv. Mater*. **2011**, *23*, 1660–1664.
9. Drees, M.; Hoppe, H.; Winder, C.; Neugebauer, H.; Sariciftci, N.S.; Schwinger, W.; Schäffler, F.; Topf, C.; Scharber, M.C.; Zhu, Z.; Gaudiana, R. Stabilization of the nanomorphology of polymer–fullerene "bulk heterojunction" blends using a novel polymerizable fullerene derivative. *J. Mater. Chem.* **2005**, *15*, 5158–5163.
10. Senkovskyy, V.; Tkachov, R.; Beryozkina, T.; Komber, H.; Oertel, U.; Horecha, M.; Bocharova, V.; Stamm, M.; Gevorgyan, S.A.; Krebs, F.C.; Kiriy, A. "Hairy" poly(3-hexylthiophene) particles prepared via surface-initiated kumada catalyst-transfer polycondensation. *J. Am. Chem. Soc.* **2009**, *131*, 16445–16453.
11. Krebs, F.C.; Senkovskyy, V.; Kiriy, A. Preorganization of nanostructured inks for roll-to-roll coated polymer solar cells. *IEEE J. Sel. Topics Quant. Electron.* **2010**, *16*, 1821–1826.
12. Tkachov, R.; Senkovskyy, V.; Horecha, M.; Oertel, U.; Stamm, M.; Kiriy, A. Surface-initiated Kumada catalyst-transfer polycondensation of poly(9,9-dioctylfluorene) from organosilica particles: Chain-confinement promoted b-phase formation. *Chem. Commun.* **2010**, *46*, 1425–1427.
13. Gupta, D.; Mukhopadhyay, S.; Narayan, K.S. Fill factor in organic solar cells. *Sol. Energy Mater. Sol. Cells* **2010**, *94*, 1309–1313.
14. Meier, C.; Gondorf, A.; Lüttjohann, S.; Lorke, A.; Wiggers, H. Silicon nanoparticles: Absorption, emission, and the nature of the electronic bandgap. *J. Appl. Phys.* **2007**, *101*, 103–112.
15. Søndergaard, R.; Strobel, S.; Bundgaard, E.; Norrman, K.; Hansen, A.G.; Albert, E.; Csaba, G.; Lugli, P.; Tornow, M.; Krebs, F.C. Conjugated 12 nm long oligomers as molecular wires in nanoelectronics. *J. Mater. Chem.* **2009**, *19*, 3899–3908.
16. Horcas, I.; Fernandez, R.; Gomez-Rodriguez, J.M.; Colchero, J.; Gomez-Herrero, J.; Baro, A.M. WSXM: A software for scanning probe microscopy and a tool for nanotechnology. *Rev. Sci. Instrum.* **2007**, *78*, 013705:1–013705:8.
17. Baldwin, R.K.; Pettigrew, K.A.; Garno, J.C.; Power, P.P.; Liu, G.-y.; Kauzlarich, S.M. Room temperature solution synthesis of alkyl-capped tetrahedral shaped silicon nanocrystals. *J. Am. Chem. Soc.* **2002**, *124*, 1150–1151.
18. Baldwin, R.K.; Pettigrew, K.A.; Ratai, E.; Augustine, M.P.; Kauzlarich, S.M. Solution reduction synthesis of surface stabilized silicon nanoparticles. *Chem. Commun*. **2002**, 1822–1823.
19. Lee, J.-L.; Kung, M.C.; Trahey, L.; Missaghi, M.N.; Kung, H.H. Nanocomposites derived from phenol-functionalized Si nanoparticles for high performance lithium ion battery anodes. *Chem. Mater*. **2009**, *21*, 6–8.
20. Chen, L.; Pan, X.; Zheng, D.; Gao, Y.; Jiang, X.; Xu, M.; Chen, H. Hybrid solar cells based on P3HT and Si@MWCNT nanocomposite. *Nanotechnology* **2010**, *21*, 345201–345211.
21. Ruckenstein, E.; Li, Z.F. Surface modification and functionalization through the self-assembled monolayer and graft polymerization. *Adv. Colloid Interface Sci.* **2005**, *113*, 43–63.

22. Andersen, T.R.; Larsen-Olsen, T.T.; Andreasen, B.; Böttiger, A.P.L.; Carlé, J.E.; Helgesen, M.; Bundgaard, E.; Norrman, K.; Andreasen, J.W.; Jørgensen, M.; Krebs, F.C. Aqueous processing of low-band-gap polymer solar cells using roll-to-roll methods. *ACS Nano* **2011**, *5*, 4188–4196.
23. Nelles, J.; Sendor, D.; Ebbers, A.; Petrat, F.M.; Wiggers, H.; Schultz, C.; Simon, U. Functionalization of silicon nanoparticles via hydrosilylation with 1-alkenes. *Colloid Polym. Sci.* **2007**, *285*, 729–736.
24. Hirschman, K.D.; Tsybeskov, L.; Duttagupta, S.P.; Fauchet, P.M.; Silicon-based visible light-emitting devices integrated into microelectronic circuits. *Lett. Nat.* **1996**, *384*, 338–341.

Supporting Information

Synthesis

A small test was made where meta-cresol was grafted onto silicon nanoparticles to investigate the grafting and the following purification. The synthesis method was:

To a solution of naphatalene (0.35 g, 2.7 mmol) in dry glyme (5 mL) sodium (0.1 g, 4.3 mmol) was added and the mixture was stirred for 3 hours after which a black yellowish solution of sodium naphatalide was obtained. This solution was added to a solution of $SiCl_4$ (99.9%, 0.08 mL, 0.7 mmol) in dry glyme (30 mL) and stirred for 30 min. The organic grafting agent (0.19 mL, 1.78 mmol) was added and stirring continued for 2 hours.

From this point on two different methods of purification was applied.

1. The solvent was removed under reduced pressure; the residue was dissolved in heptane and washed with water. The organic phases were collected and the solvent was removed under reduced pressure, the residue was heated to 90 °C to remove residual naphthalene and meta-cresol resulting in a yellowish solid.
2. The solvent was removed under reduced pressure. When all the solvent was removed the temperature was increased to 90 °C to remove residual naphthalene and meta-cresol resulting in a yellowish solid.

NMR Spectra

Figure S1. NMR-spectra of meta-cresol and the two different way of purification with and without water.

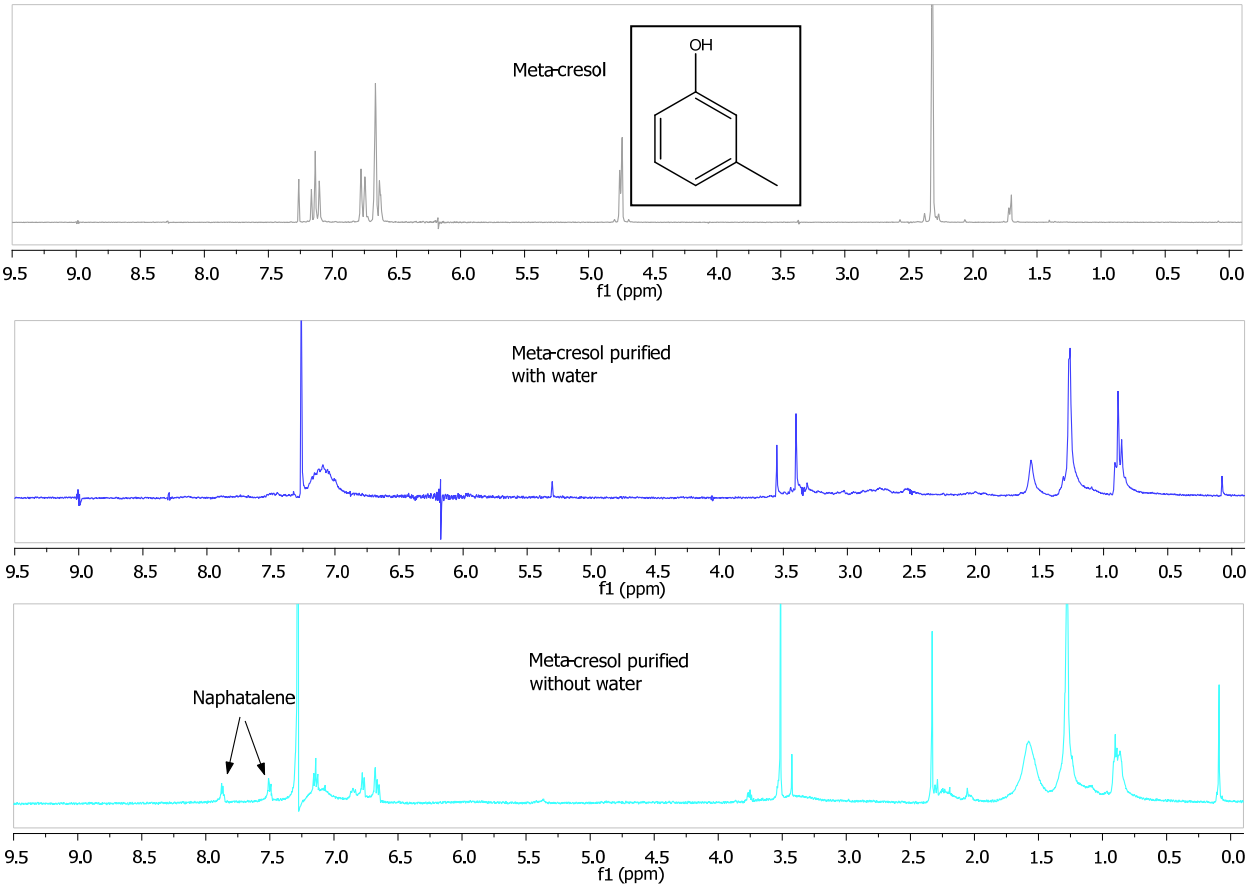

UV-Vis

Figure S2: Absorption spectra of Silicon nano-particles capped with butyl in hexane.

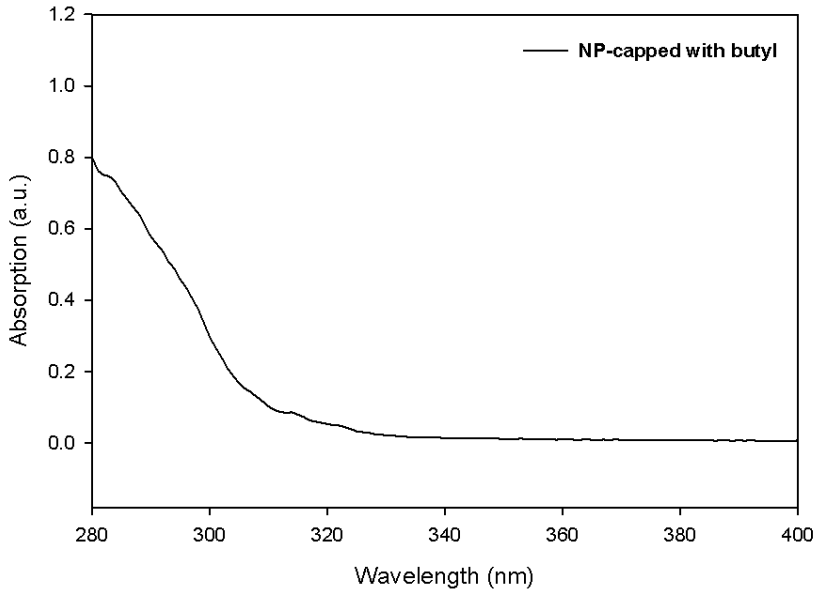

IV-Curves

Figure S3. I-V curves of unannealed and annealed devices prepared with **2** and **NP2** with [60]PCBM.